Investigating the mechanism of earthquakes in the Iranian plateau using the GCMT catalogue

۱- مهدی رضاپور – عضو هیات علمی دانشگاه تهران ، رتبه استاد
Mehdi Rezapour, rezapour@ut.ac.ir

نویسنده مسئول

۲- نسرین رضائی- دانشجوی کارشناسی ارشد زلزله شناسی
Nasrin Rezaei, rezaei.n@ut.ac.ir

Abstract

Routine estimates of the seismic moment (M_0) by the Global Centroid Moment Tensor Project (GCMT) for large and moderate earthquakes, provide a valuable resource for tectonic analysis. In this research, the source type of 614 earthquakes that occurred in the Iranian plateau between 1676 and 2023, whose moment tensor solutions are available in the GCMT catalogue, was investigated. Here, earthquakes are grouped according to dip angle values of the *T*, *P*, and *B* axes which were taken from GCMT catalogue. The mechanism is considered as strike-slip or normal faulting when dip angle of the *B* or *P* axes exceeds 60° respectively. When the dip angle of *T* axis exceeds 50° the mechanism is proposed as thrust faulting. The focal mechanism study of 614 earthquakes showed that about 55.4, 25.4 and 2.9 percent of them have reverse, strike-slip and normal mechanisms, respectively. The average value equal to 0.12 for f_{CLVD} values of 614 earthquakes shows that the non-double-couple component in the their deviatoric tensors is very small. Also, comparison of seismic moment estimated for 182 earthquakes by IRSC and GCMT, shows that there is an almost systematic bias in the seismic moment estimated by IRSC. Seismic moment values reported by IRSC are lower than those determined by GCMT.

Keywords: Focal mechanism, moment tensor, GCMT catalogue, Iranian plateau, IRSC

1. Introduction

The formation of various Tethys basins, caused the fragmentation and separation of the supercontinents of Eurasia, Gondwana (~510 M years), blocks and subplates between them. In the Middle Cambrian Epoch, during the third stage of breaking apart of the most recent supercontinent of Pangaea (~335 M years) the Paleo-Tethys Ocean began to open (Zhai, et al, 2015). The collision of the Indian and Asian plates in the Triassic period caused the closure of the Paleo-Tethys Ocean and the formation of the Alpine-Himalayan orogenic belt. The Iranian plateau is one of the most complex geodynamic settings within the Alpine-Himalayan orogenic belt, is a high land that includes a part of the Eurasian plate and a small part of the Arabian plate.

The plateau of Iran consists of several structural units, each of which has a relatively unique characteristic in terms of orogenic and tectonic events, stratigraphic and geological style. The Alborz and Zagros Mountain ranges forms a large part of the Iranian plateau. The genesis of the rift during the main fracture of the Zagros is related to the creation of the Neotethys in the south and the closure of the Paleotethys in the north of Iran (Alborz Mountain range) which caused by the Hercynian orogeny phase in the Turan plate (Stöcklin, 1968). The PaleoThetys and NeoThetys ocean subduction are responsible for the formation several magmatic arcs and sedimentary basin zones within the Iranian plateau (Stampfli and Borel, 2002). These zones are separated from each other by thrust faults that display the ancient suture zones and ophiolite belts (Berberian and King, 1981; Richards, 2015).

The structural pattern and kinematics of active deformation in the region is controlled by a combination of interplaying tectonic forces governing over the Arabian–Eurasian convergence zone, due to extending a divergent boundary through the Red Sea and the Gulf of Aden (Fig. 1). Therefore, the convergence of the Eurasian and Arabian plates causes deformation and earthquakes in the Iranian plateau. The deformation in northwest Iran is characterized by right-lateral movement at a velocity of 8 mm/year on the North Tabriz Fault, which is in agreement with recurrence period of 250–300 years suggested by seismicity studies (Masson et al., 2006). Estimate deformation based on GPS and gravity observations in the Alborz Mountain range suggest that the eastern Alborz mainly accommodates strike slip deformation (~5 mm yr^{-1}), and that the western Alborz accommodates thrusting (~6 mm yr^{-1}) (Djamour, et al, 2010). Also, the transversal NE trending shortening rate in the fold-and-thrust belt of Zagros increases from NW to SE and reaches about 10 mm yr^{-1} near its southeastern edge (Vernant et al., 2004). The velocity filed study in the Iranian plateau using GPS measurements by Mousavi et al (2013) showed that the present-day northward motion decreases eastward from 11 mm yr^{-1} at (~52°E) to 1.5 mm yr^{-1} at Mashhad (~60°E), and N–S shortening across the Kopeh Dagh, Binalud and Koh-e-Sorkh ranges sums to 4.5±0.5 mm yr^{-1} at longitude 59°E.

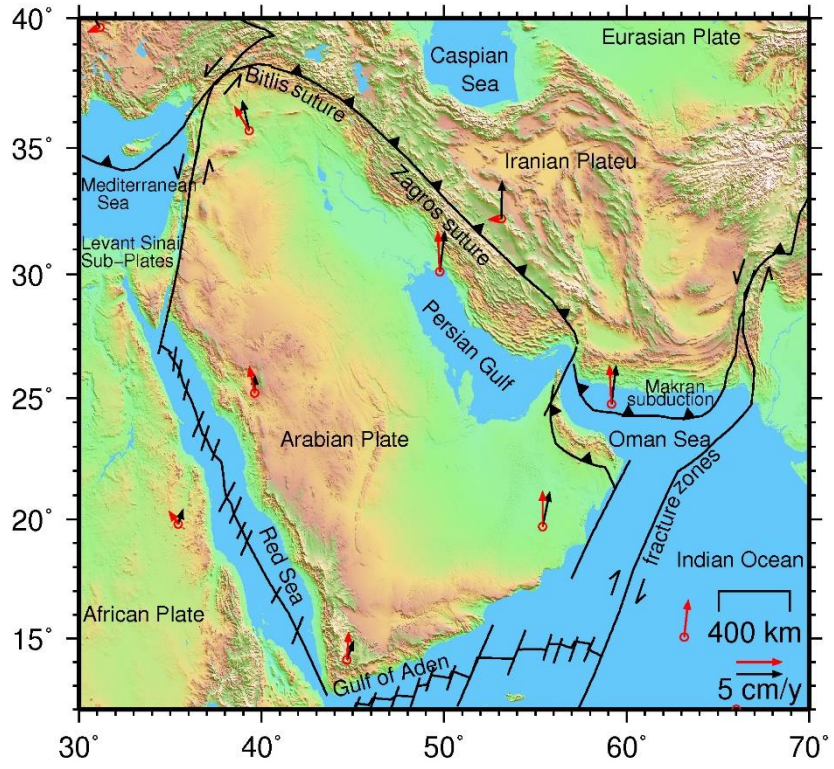

Figure 1. Tectonic map of the region, including major fault zones (black lines, after Al-Lazki et al. 2002). The red and black vectors present the absolute and relative motion of plate, respectively (after, Al-Lazki et al. 2002).

Plotting the beach ball at the central location or another location on the map with an arrow connecting the beach ball and the epicenter is one of the most common ways to express earthquake focal mechanism. But it is difficult to show the mechanism of large number of earthquakes with different mechanisms by beachballs on map. A ternary plot or triangle plot is a barycentric plot on three variables. It graphically depicts the ratios of the three variables as positions in an equilateral triangle. It is used in different sciences such as petrology, mineralogy, and etc. to show the compositional data in the three-dimensional case. Seismologists also use this diagram to display similarity and diversity of earthquake focal mechanisms. Triangle diagrams were first used to plot earthquake mechanisms by Apperson and Frohlich (1988) and Frohlich and Apperson (1992). Álvarez-Gómez, (2019) used a ternary plot by presenting the software FMC (Earthquake focal mechanisms data management, cluster and Classification). In this study, the mechanism of earthquakes occurred in the plateau of Iran is investigated using the triangular diagram and the Global Centroid Moment Tensor (GCMT) catalogue.

2. Data and processing

Global CMT catalogue was used in this study. One of the common methods of studying the geodynamics of a region is to determine the seismic moment tensor of earthquakes that occurred in that region. While the pioneering studies to determine the seismic moment occurred in the late

1960s and in the early 1970s, the Harvard CMT method of Dziewonski and Woodhouse (1983) became a common systematic determination of earthquake moment tensors.

Routine estimates of the seismic moment (M_0) by the Harvard group as Centroid Moment Tensor (CMT) solutions developed and maintained as an extensive catalogue for most earthquakes above $m_b \approx 5.0$ over the period 1976-2006. Since then, it is maintained and continued by the Global Centroid Moment Tensor Project (GCMT) at the Lamont-Doherty Earth Observatory (LDEO) of Columbia University. The completeness of catalogue and accuracy vary both geographically and through time, and depend on earthquake depth and tectonic environment. The Harvard group have utilized long-period (45-200 sec) body and surface waves (for very large earthquakes) to determine scalar moments and moment tensors.

In the GCMT catalogue, for each earthquake the available parameters are: origin time, epicentral coordinates, reported magnitude; data used in the CMT inversion; type of source inverted for CMT; type and duration of moment-rate function assumed in the inversion; centroid parameters determined in the inversion; scalar moment value, the moment-tensor elements; eigenvalues, plunge, and azimuth of the three eigenvectors; strike, dip, and rake of nodal planes; etc. The moment tensor is specified by determining the trend and plunge of its *T*, *P*, and *B* axes (eigenvectors), and the values of its three principal moments (eigenvalues). The *T*, *P*, and *B* axes are the principal axes associated with the largest, smallest, and intermediate principal moment values (m_T, m_P, m_B), respectively.

The source type can be determined using the orientation of the principal axes of the moment tensor. For earthquakes on the normal, reverse, and strike-slip faults, the *P*, *T*, and *B* axes are near vertical, respectively. Therefore, we have pure reverse mechanism when δ_T is 90°, pure normal mechanism when δ_P is 90°, and pure strike-slip mechanism when δ_B is 90° (Fig. 2). In this figure each beach ball which has been plotted within triangle vertices indicate pure normal mechanism on a 45° dipping fault, pure reverse mechanism on a 45° dipping fault, and pure strike-slip mechanism on a vertical fault. In other words, the mechanisms plotted at the vertices of the triangle represent the slip along the strike of fault or in the direction of the fault slope. Other beach balls in Figure 2 show mechanisms of faulting with combined horizontal and vertical movement. Triangle diagram practically determine the fraction of dip-slip (reverse or normal) and strike-slip components of an earthquake.

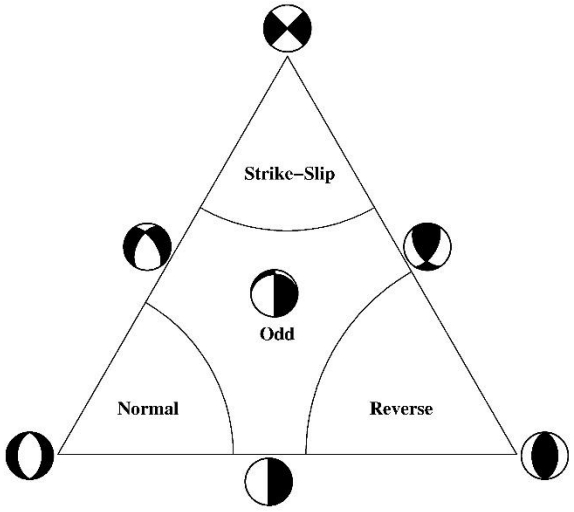

Figure 2. The three vertices correspond to pure normal, reverse, and normal mechanisms. The curved lines on the figure correspond to mechanisms having *P* and *B* axes with dips of 60°, and a *T* axis with a dip to 50° (Frohlich and Apperson, 1992). For an earthquake with T, P, and B axes having dip angles relative to horizontal of δ_T, δ_P, and δ_B, the proportion of the reverse, normal, and strike slip mechanisms are $\sin^2 \delta_T$, $\sin^2 \delta_P$, and $\sin^2 \delta_B$, respectively. Therefore, we have $\sin^2 \delta_T + \sin^2 \delta_P + \sin^2 \delta_B = 1$, which is equation of sphere. Plotting source mechanism on the triangle diagram is equivalent to the cartographer's problem of projecting locations from a quarter hemisphere onto a triangle flat surface. This map projection is the azimuthal gnomonic projection (Richardus and Adler, 1972).

Earthquakes whose locations are in the range of latitude 24° to 40° and longitude 44° to 63° were extracted from GCMT catalogue. In this way, 614 earthquakes that occurred between 1967 and 2023 were extracted. The researchers classified the earthquake mechanism based on the plunge of the stress axes of *T*, *P*, and *B* (Frohlich and Apperson (1992); Zoback, (1992); Johson et al. (1994); Frohlich, (2001)). Frohlich and Apperson (1992), Zoback, (1992) and Johson et al. (1994) have classified the earthquake mechanism into 4, 7 and 8 groups, respectively. Álvarez-Gómez, (2019) has used the classification of Johnson et al. (1994) in his FMC software. Therefore, the focal mechanism of an earthquake can be studied using the dip angle of eigenvectors ($\delta_T, \delta_P, \delta_B$).

Nouri-Delouei and Ghaitanchi (2021a, 2021b) studied the classification of earthquakes mechanism in the Iran plateau using FMC software. They classified the mechanism of earthquakes into 7 groups. Here, following Frohlich and Apperson (1992), earthquakes are grouped in 4 groups according to dip angle values of the *T*, *P*, and *B* axes which were taken from GCMT catalogue. In Figure 3 focal mechanisms of these 614 earthquakes are displayed on a triangle diagram. Figure 3 shows that both reverse and strike slip mechanisms are common in Iranian plateau, but the reverse mechanism predominate. About 55.4, 25.4 and 2.9 percent of all earthquakes shown in figure 3 are reverse, strike-slip, and normal mechanisms, respectively. Also, the remaining 16.3% of earthquakes have an odd mechanism, that is, a combination of three mechanisms: reverse, strike-slip, and normal. Epicentral distribution of 614 earthquakes are shown in Figure 4.

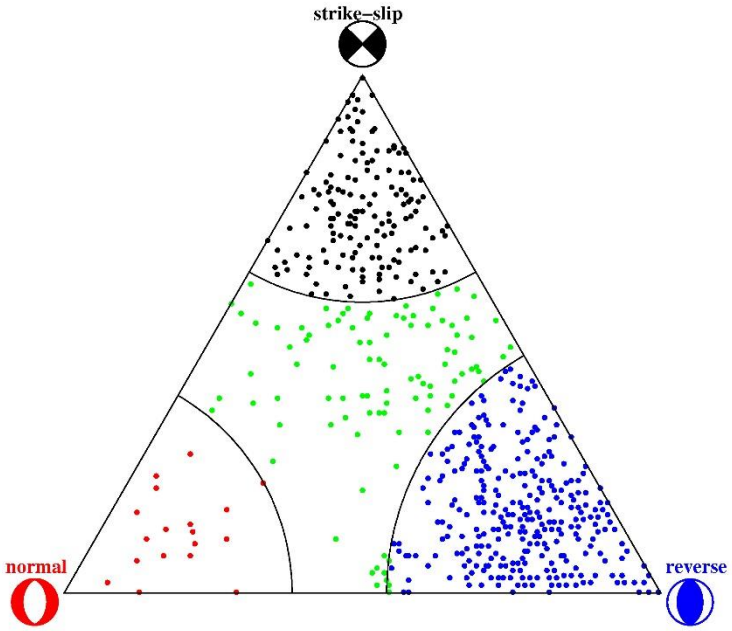

Figure 3. Triangle plot for extracted earthquakes from GCMT catalogue. These earthquakes have occurred in the Iranian Plateau during 1967 to 2023. In the set of 614 earthquakes, 340, 156, 18, and 100 earthquakes have reverse, strike-slip, normal, and odd mechanisms, respectively.

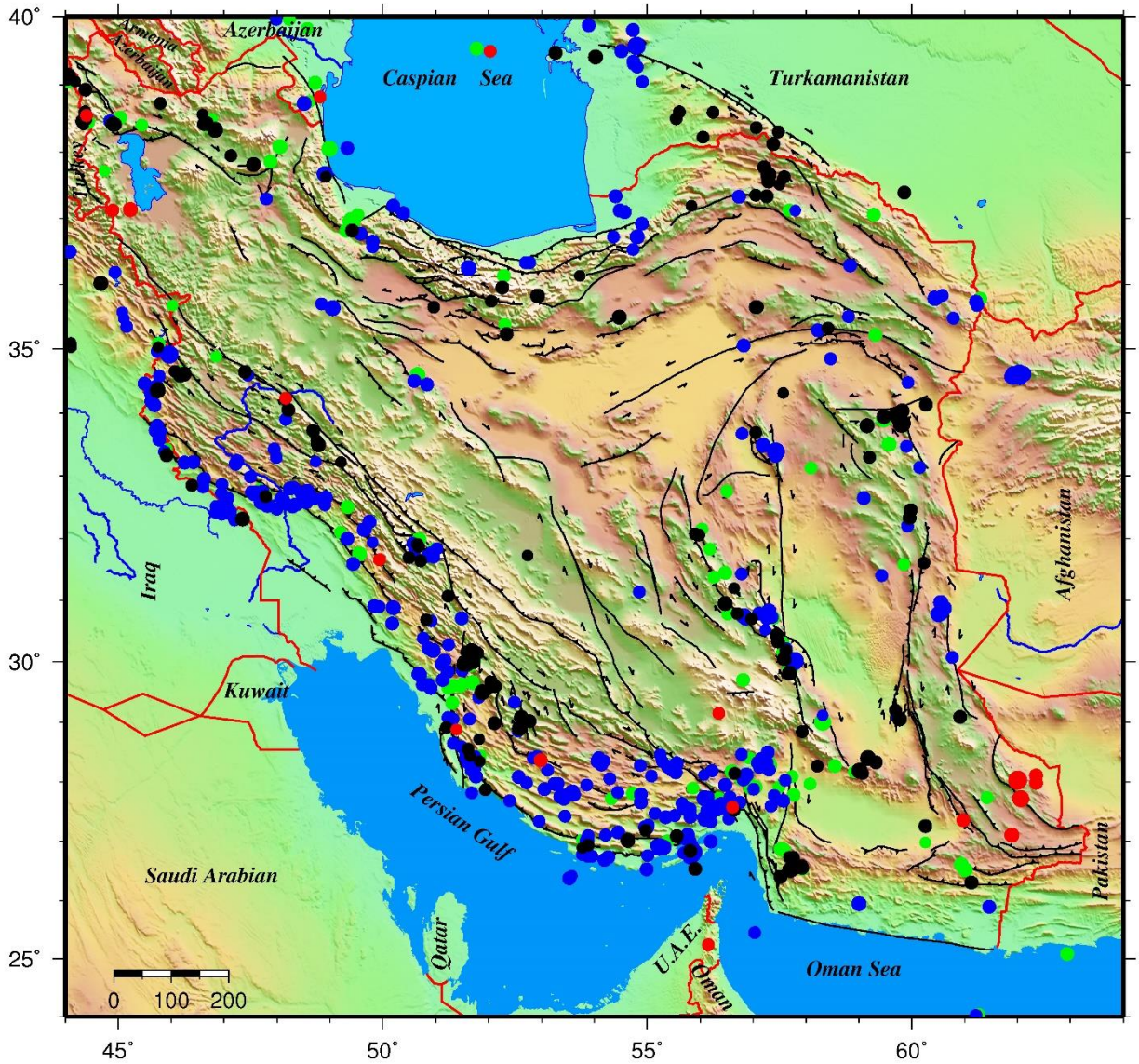

Figure 4 shows the spatial distribution of earthquakes. The blue, black, and red circles show the epicenters of events with reverse, strike slip and normal mechanisms. The green circles present the events with odd mechanisms. All of the events are scaled according to their magnitude. The solid lines show traces of major active faults in the region which were mapped by Hessami et al., 2003.

As we expect, the earthquakes occurring in the Zagros Mountain range have a reverse mechanism. Due to the location of the Iranian Plateau in the Eurasian-Arabian Collision Zone, earthquakes with a reverse mechanism are dominant. Earthquakes with a strike-slip mechanism are also common. But, events with normal mechanisms are very few. The occurrence of earthquakes with a combined mechanism shows the complexity of the region in terms of geodynamics.

Histograms of hypocentral and centroid depth values for 614 selected earthquakes are compared in Figure 5. Hypocentral depth is determined using arrival times of P and S phases, while centroid depth is determined by seismic wave inversion. The location of the hypocenter is at the point where rupture is initiated, while the centroid is the location across the fault surface where slip is dominant.

The centroid location coincided with the area where the maximum surface ruptures were observed. As figure 5 shows, hypocentral-depth values of 10 and 33 km in the GCMT Catalogue are dominated by artificial effects such as fixing for negative or unstable values and probably as starting depth in inversion routine. Also, centroid depth values of 12, 15, and 33 km are dominated by artificial effects. The values of 12 or 15 km and 33 km are probably corresponded to the average Conrad and Moho discontinuities. The routine GCMT procedures and algorithms are not expected to provide a depth resolution better than about 10–15 km for shallow earthquakes (Engdahl et al.2006).

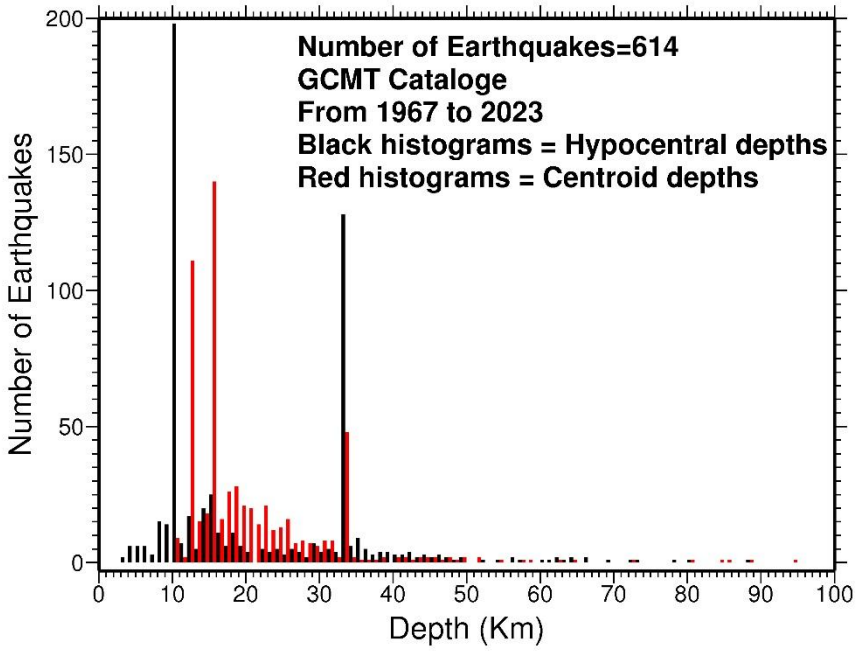

Figure 5. Histograms comparing hypocentral depths (black) with centroid depths (red) for 614 earthquakes in GCMT catalogue which occurred in the Iranian plateau.

The seismic energy radiated from a fault can be modeled with a double-couple source, the equivalent body-force representation of the displacement field. A moment tensor with nonzero isotropic component represents a volume change. The moment tensor computed from seismic data may include contributions from other type of sources. It can be decomposed into isotropic and deviatoric parts, $M = M^I + M^D$. The deviatoric moment tensor is free of any isotopic sources but may contain additional non-double-couple component, $M^D = M^{DC} + M^{CLVD}$. The non-double-couple component called *compensated liner vector dipoles* (*CLVDs*). These are sets of three force dipoles that are compensated, with one dipole -2 times the magnitude of the others. The trace in the *CLVD* is zero. Moment tensors estimated from waveform inversion rarely correspond to pure double couples. The estimate moment tensor can be decomposed into a major and minor double couple or into a major double couple and a *CLVD*. When there is a uniform inward/outward motion in a plane a *CLVD* source occurs, according to shortening/expansion normal to the plane.

We can to identify the type of source by examining eigenvalues of moment tensor. In an ideal explosion, all of the eigenvalues are equal, none are zero. In a double-couple source two

eigenvalues are equal in magnitude and opposite in sign, the third is zero. Frohlich and Apperson (1992) have proposed a way to express the non-double couple component of moment tensors as

$$f_{CLVD} = \frac{min(|m_T|, |m_P|, |m_B|)}{max(|m_T|, |m_P|, |m_B|)} = \frac{|m_B|}{max(|m_T|, |m_P|)}$$

Where m_T, m_B and m_P are the largest, intermediate, and smallest principal moments, respectively. The f_{CLVD} i.e., compensated linear vector dipole ratio measures how different the source is from a pure double couple source. The f_{CLVD} is equal zero in a pure double-couple source, and it is equal 0.5 in a pure *CLVD* source. We expect to observe a minor *CLVD* component in the inversion of the moment tensor due to inaccurate propagation corrections which attributed to the noise. Some events have a *CLVD* value larger than expected to be caused by noise.

While Harvard group in the routine earthquake modeling, due to stability of modeling, include a constrain that the isotropic component equals zero, they do not constrain the CMT solutions to be pure double-couples (Ammon et al, 2021). Therefore, many earthquakes have a substantial *CLVD* component. Figure 5 shows the histogram of f_{CLVD} values for 614 earthquakes which occurred in the Iranian plateau. The mean of f_{CLVD} values for 614 earthquakes in the CMT catalogue which occurred in Iranian plateau is 0.12. Moment tensor of sources such as opening a crack under tension, inflating magma dike in volcanic areas, deep earthquakes, and near-simultaneous earthquakes on nearby faults of different geometries have a large *CLVD* component, but they are rare. More than one physical mechanism is required to explain the observed varieties of non-double-couple earthquakes. The simplest explanation is that some earthquakes are complex, with stress released on two or more suitably oriented, nonparallel fault surfaces (Frohlich, 1994). The *CLVD* components reflect complexities in the earthquake source, e.g., irregularly shaped faults, seismic anisotropy, shear-tensile faulting induced by fluid injection in volcanic or geothermal areas, or the presence of a material interface in the focal zone (Frohlich, 1994; Vavryčuk and Hrubcová 2017).

In a deviatoric source the deviation from a pure double-couple is given by the percentage of *CLVD* present, by the $200 \times f_{CLVD}$. For an earthquake with $f_{CLVD} = 0.25$, about 50% of its moment is *CLVD* component. As Figure 6 shows, only 12.4% of the used dataset has *CLVD* value greater or equal 0.25 in the estimated moment tensors.

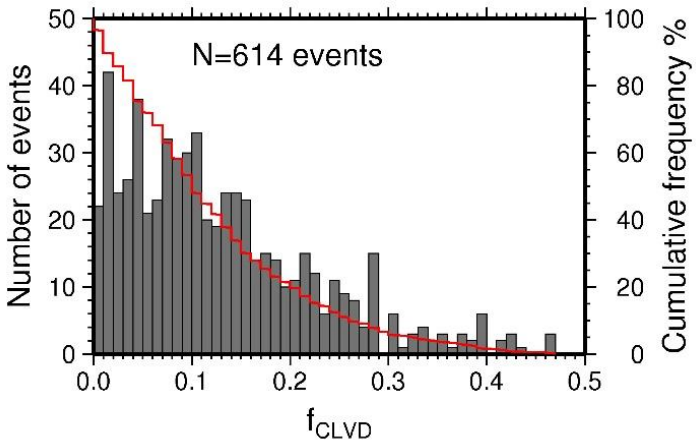

Figure 6. Histogram of f_{CLVD} values in bins with width 0.01, for earthquakes occurring between 1976 and 2023, in the Iranian plateau. A measure often quoted is 200×f_{CLVD}, which is the percent non-double component. The red-line and right axis present the cumulative frequency of f_{CLVD} values.

3. Comparison GCMT and IRSC catalogues

As mentioned before, the Harvard group reported Centroid Moment Tensor (CMT) solutions for earthquakes with $m_b \geq 5.0$, during 1976 to 2006. Since then, it is maintained and continued by the Global Centroid Moment Tensor Project (GCMT) at Columbia University. Iranian Seismological Center (IRSC) reports the moment tensor solution for moderate and large earthquakes which occurred in the Iranian plateau, since 2012. IRSC applies the ISOLA, ISOLated Asperities software package (Sokos and Zahradník 2008, 2013) to local and regional waveforms to perform moment tensor inversion (Hosseini et al, 2019). Hosseini et al. (2019) published the seismic moments of 194 earthquakes as IRSC catalogue. They compared the seismic moments of 111 events in the IRSC and GCMT catalogues and concluded that the values of the seismic moments in the IRSC catalogue are underestimated compared to the values published in the GCMT catalogue. In this study, comparison IRSC and GCMT catalogues shows that for 182 earthquakes which occurred in the Iranian plateau, their moment tensor solutions are available in both catalogues. Also, Ahmadzadeh and Javan (2024) recently published focal mechanism of 64 earthquakes which occurred in Alborz region. They collected all available focal mechanism for which the quality of solutions could be determined in order to construct a focal mechanism catalogue for the Alborz region. Here estimated source parameters such as seismic moment, hypocentral and centroid depth are compared for two catalogues (Fig.7).

Figure 7 shows the comparison of seismic moment estimated by IRSC and GCMT. This figure indicates that there is an almost systematic bias in the seismic moment estimated by IRSC. Seismic moment values reported by IRSC are lower than those determined by GCMT. For this difference various reasons such as type of data (local, regional, or teleseismic), the velocity model (local or global), different frequency band, and incorrect seismometer response in the process of inversion can be mentioned. IRSC uses a local velocity model and local/regional data, while in the GCMT

project the teleseismic data and the global velocity model of PREM (Dziewonski and Anderson, 1981) are used.

Also, the hypocentral and centroid depth reported in both catalogues are compared in Figure 8.

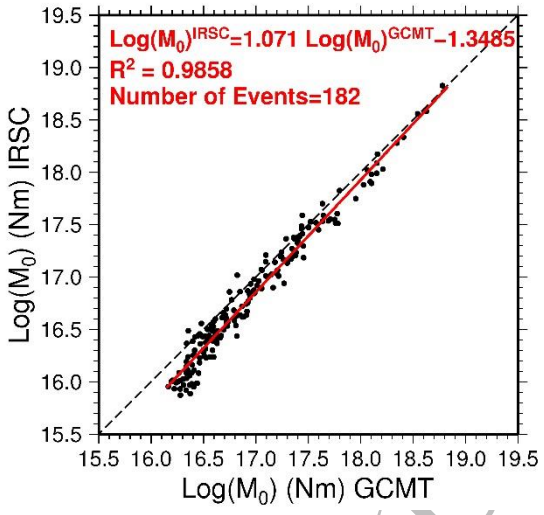

Figure 7. Relation between seismic moment values for 182 earthquakes reported by IRSC and GCMT from 2012 to 2023. The regression line is shown by a red line.

As Figure 8a shows, hypocentral-depth value of 10 and centroid depth value of 12 km in the GCMT Catalogue are dominated by artificial effects. In the set of 182 earthquakes that were compared, for 89 earthquakes the GCMT reported a hypocentral depth value of 10 km. Also, in this dataset the lowest centroid depth in the GCMT catalogue is 12 km, and this value has been reported for 49 earthquakes (Fig.8b). Figure 8b shows that, the CMT depth tends to be larger than the IRSC depth. The source inversion process is sensitive to the various choices that must be made regarding dataset, earth model and inversion strategy. These observed discrepancies in the estimated depth values may be related to the Earth models which Harward group (CMT) and IRSC use in their depth determinations. In the CMT the PREM model is used. IRSC uses a local structural velocity model.

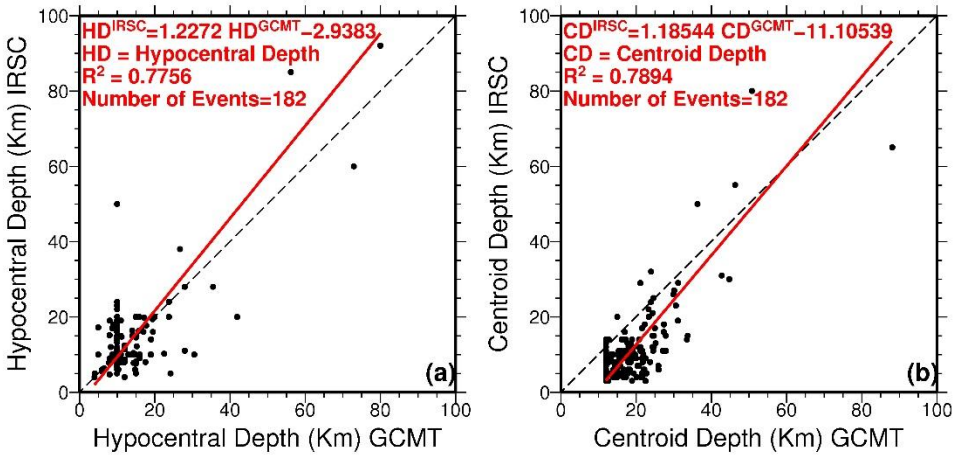

Figure 8. Relation between depth values for 182 earthquakes reported by IRSC and GCMT from 2012 to 2023. (a) For hypocentral depth. (b) For centroid depth. In each case, the regression line is shown by a red line. R = correlation coefficient.

4 Conclusion

In this paper we applied the ternary plot to evaluate the distribution of focal mechanism orientations of groups of earthquakes. The method was applied to 614 earthquakes that occurred in the Iranian plateau between 1976 and 2023, whose moment tensor solutions are available in the GCMT catalogue. Here, following Frohlich and Apperson (1992), the source type of earthquakes grouped according to dip angle values of the *T*, *P*, and *B* axes which were taken from GCMT catalogue. The applied method demonstrates that 55.4, 25.4 and 2.9 percent of earthquakes have reverse, strike-slip, and normal mechanisms; however, there is a significant portion (16.3 %) that have mechanisms which plot in the center of the triangle diagram, well away from the reverse, strike-slip, or normal vertices (Fig. 3).

While the routine earthquake modeling in the Global Centroid Moment Tensor Project (GCMT), due to stability of modeling, include a constrain that the isotropic component equals zero, the CMT solutions are not constrained to be pure double-couples. Therefore, many earthquakes have a substantial *CLVD* component. Among the best determined 614 moment tensors for earthquakes in the Iranian plateau, only 12.4% has *CLVD* value greater or equal 0.25.

Also, comparison of seismic moment estimated for 182 earthquakes by IRSC and GCMT, shows that there is an almost systematic bias in the seismic moment estimated by IRSC. Seismic moment values reported by IRSC are lower than those determined by GCMT.

Acknowledgment

All data used in this study were extracted from web sites of seismological centres: Iranian Seismological Centre (IRSC); Global Centroid Moment Tensor (GCMT). I am grateful for their contributions to this research. The figures were prepared using Generic Mapping Tools (Wessel and Smith 1998).

References

Ahmadzadeh, S., and Javan-Doloei, Gh. (2024). The high-frequency decay parameter Kappa (κ) in the Alborz Region using broadband seismic waveforms. *Journal of Seismology*. 1-18. 10.1007/s10950-024-10256-x.

Ammon, C.J., Velasco, A.A., Lay, T., and Wallace, T. (2021). Foundations of Modern Global Seismology, Elsevier, Academic Press.

Al-Lazki, A., Seber, D., and Sandvol, E. (2002). A crustal transect across the Oman Mountains on the eastern margin of Arabia. *GeoArabia*, 7, 47-78.

Álvarez-Gómez, J. A., (2018). FMC—Earthquake focal mechanisms data management, cluster and classification. *SoftwareX*, 9, 299-307.

Apperson, K. D., and Frohlich, C. (1988). The effect of the plate boundary on average earthquake focal mechanisms in convergent margins, *Geol. Soc., Abstr. Programs, 20,* A236.

Berberian, M., and King, G.C.P. (1981). Towards a paleogeography and tectonic evolution of Iran. *Can. J. Earth Sci.* 18, 210–265.

Engdahl E.R., Jackson J.A., Myers S.C., Bergman E.A., Priestley K. (2006). Relocation and assessment of seismicity in the Iran region, *Geophys. J. Int.*, 167, 761–778.10.1111/j.1365-246X.2006. 03127.x

Dziewonski, A.M., and Anderson, D.L., (1981). Preliminary reference Earth model. *Phys. Earth Planet. Inter.* 25 (4), 297–356.

Dziewonski, A. M. and Woodhouse, J.H. (1983). An experiment in systematic study of global seismicity: Centroid-moment tensor solutions for 201 moderate and large earthquake of 1981, *J. Geophys. Res., 88,* 3247-3271.

Djamour, Y., Vernant, P., Bayer, B., Nankali, H.R., Ritz, J.F., Hinderer, J., Hatam, Y., Luck, B., Moigne, L.N., Sedighi, M., and Khorrami, F. (2010) GPS and Gravity Constraints on Continental Deformation in the Alborz Mountain Range, Iran. *Geophys. J. Int*, 183, 1287-1301. https://doi.org/10.1111/j.1365-246X.2010.04811.x

Frohlich, C. (1992). Triangle diagrams ternary graphs to display similarity and diversity of earthquake focal mechanisms. *Phys Earth Planet Inter*, 75 193-198.

Frohlich, C. (1994) Earthquakes with non-double-couple mechanisms, *Science*, 264(5160), 804-809.

Frohlich, C and Apperson, K. D. (1992). Earthquake focal mechanisms, moment tensors, and the consistency of seismic activity near plate boundaries. *Tectonics*, 11 279-296

Hessami, K., Jamali, F., Tabassi, H. (2003). Major active faults of Iran, scale 1:25,000,000. Ministry of Science, Research and Technology, International Institute of Earthquake Engineering and Seismology, Iran.

Hosseini, H., Pakzad, M., and Naserieh, S., (2019). Iranian regional centroid moment tensor catalogue: Solutions for 2012–2017. *Phys. Earth Planet. Inter*., 286, 29-41.

Masson, F., Djamour, Y., Van-Gorp, S., Chery, J., and Tatar, M., Tavakoli, F., Nankali, H. and Vernant, P. (2006). Extension in NW Iran driven by MW 6.5, 6.4 Ahar-Varzghan doublet earthquakes 1203 the motion of the South Caspian Basin. *Earth and Planetary Science Letters, 252*, 180–188.

Mousavi, Z., Walpersdorf, A., Walker, R.T., Tavakoli, F., Pathier, E., Nankali, H., Nilfouroushan., F., and Djamour, Y. (2013). Global Positioning System constraints on the active tectonics of NE Iran and the South Caspian region, *Earth and Planetary Science Letters, 377-378,* 287–298.

Nouri-Delouei, M., and Gheitanchi, M.R., (2021a). Fault mechanisms and their frequencies during destructive earthquakes in Iran. *Tectonics Journal*, 5, 91-102.

Nouri-Delouei, M., and Gheitanchi, M.R., (2021b). Classification of Zagros earthquakes based on focal mechanism. *Contributions to Geophysics and Geodesy*, 51, 265-275.

Richards, J.P. (2015) Tectonic, magmatic, and metallogenic evolution of the Tethyan orogen: From subduction to collision, *Oro Geology Reviews*, 70, 323-345.

Richardus, P. and Adler, R.K. (1972). Map Projections North Holland, Amsterdam, 174 pp.

Stöcklin, J. (1968). Structural history and tectonics of Iran, a review, *Am. Assoc. Pet. Geol. Bull*., 52, 1229–1258.

Stampfli, G.M., Borel, G.D. (2002). A plate tectonic model for the Paleozoic and Mesozoic constrained by dynamic plate boundaries and restored synthetic oceanic isochrons. *Earth Planet. Sci. Lett.* 196, 17–33.

Sokos, E. and Zahradník, J. (2008). ISOLA – A Fortran code and a Matlab GUI to perform multiple-point source inversion of seismic data, *Comput. Geosci*., 34, 967–977.

Sokos, E. and Zahradník, J. (2013). Evaluating Centroid-Moment-Tensor Uncertainty in the New Version of ISOLA Software, *Seismological Research Letters*, 84, 656-665.

Vavryčuk, V., and Hrubcová, P. (2017) Seismological evidence of fault weakening due to erosion by fluids from observations of intraplate earthquake swarms, *J. Geophys. Res*., 122, doi.org/10.1002/2017JB013958

Vernant, P., Nilforoushan, F., Hatzfeld, D., Abbasi, M. R., and Vigny, C. (2004). Contemporary crustal deformation and plate kinematics in Middle East constrained by GPS measurements in Iran and northern Oman. *Geophys. J. Int*, 157, 381–398.

Zhai, Q. G., Jahn, B. M., Wang, J., Hu, P. Y., Chung, S. L., Lee, H. Y., Tang, S. H., and Tang, Y. (2015). "Oldest Paleo-Tethyan ophiolitic mélange in the Tibetan Plateau". *Geological Society of America Bulletin.* 128 (B31296-1): 355–373. doi:10.1130/B31296.1

Zoback, M.L., (1992). Stress Field Constraints on Intraplate Seismicity in Eastern North America. *J. Geophys. Res*. 92, 11761-11782.